Electrostatic actuation of silicon optomechanical resonators

Suresh Sridaran[1,*] and Sunil A. Bhave[1,2]

[1]*OxideMEMS Lab, School of Electrical and Computer Engineering, Cornell University, Ithaca, New York 14853, USA*
[2]*sunil@ece.cornell.edu*
*ss625@cornell.edu

Abstract: Cavity optomechanical systems offer one of the most sensitive methods for detecting mechanical motion using shifts in the optical resonance frequency of the optomechanical resonator. Presently, these systems are used for measuring mechanical thermal noise displacement or mechanical motion actuated by optical forces. Electrostatic capacitive actuation and detection have been shown previously for silicon micro electro mechanical resonators for application in filters and oscillators. Here, we demonstrate monolithic integration of electrostatic capacitive actuation with optical sensing using silicon optomechanical disk resonators and waveguides. The electrically excited mechanical motion is observed as an optical intensity modulation when the input electrical signal is at a frequency of 235MHz corresponding to the radial vibrational mode of the silicon microdisk.

©2011 Optical Society of America

OCIS codes: (120.4880) Optomechanics; (130.4110) Modulators; (230.4685) Optical microelectromechanical devices.

References and links

1. A. Schliesser, O. Arcizet, R. Rivière, G. Anetsberger, and T. J. Kippenberg, "Resolved-sideband cooling and position measurement of a micromechanical oscillator close to the Heisenberg uncertainty limit," Nat. Phys. **5**(7), 509–514 (2009).
2. T. J. Kippenberg and K. J. Vahala, "Cavity opto-mechanics," Opt. Express **15**(25), 17172–17205 (2007).
3. G. S. Wiederhecker, L. Chen, A. Gondarenko, and M. Lipson, "Controlling photonic structures using optical forces," Nature **462**(7273), 633–636 (2009).
4. J. Rosenberg, Q. Lin, and O. Painter, "Static and dynamic wavelength routing via the gradient optical force," Nat. Photonics **3**(8), 478–483 (2009).
5. M. Li, W. H. P. Pernice, C. Xiong, T. Baehr-Jones, M. Hochberg, and H. X. Tang, "Harnessing optical forces in integrated photonic circuits," Nature **456**(7221), 480–484 (2008).
6. H. Rokhsari, T. J. Kippenberg, T. Carmon, and K. J. Vahala, "Radiation-pressure-driven micro-mechanical oscillator," Opt. Express **13**(14), 5293–5301 (2005).
7. M. Eichenfield, R. Camacho, J. Chan, K. J. Vahala, and O. Painter, "A picogram- and nanometre-scale photonic-crystal optomechanical cavity," Nature **459**(7246), 550–555 (2009).
8. M. Tomes and T. Carmon, "Photonic micro-electromechanical systems vibrating at X-band (11-GHz) rates," Phys. Rev. Lett. **102**(11), 113601 (2009).
9. S. Gigan, H. R. Böhm, M. Paternostro, F. Blaser, G. Langer, J. B. Hertzberg, K. C. Schwab, D. Bäuerle, M. Aspelmeyer, and A. Zeilinger, "Self-cooling of a micromirror by radiation pressure," Nature **444**(7115), 67–70 (2006).
10. J. D. Thompson, B. M. Zwickl, A. M. Jayich, F. Marquardt, S. M. Girvin, and J. G. E. Harris, "Strong dispersive coupling of a high-finesse cavity to a micromechanical membrane," Nature **452**(7183), 72–75 (2008).
11. J. Wang, Z. Ren, and C. T.-C. Nguyen, "1.156-GHz self-aligned vibrating micromechanical disk resonator," IEEE Trans. Ultrason. Ferroelectr. Freq. Control **51**(12), 1607–1628 (2004).
12. J. R. Clark, W.-T. Hsu, M. A. Abdelmoneum, and C. T.-C. Nguyen, "High-Q UHF micromechanical radial-contour mode disk resonators," J. Microelectromech. Syst. **14**(6), 1298–1310 (2005).
13. S. Pourkamali, Z. Hao, and F. Ayazi, "VHF single crystal silicon capacitive elliptic bulk-mode disk resonators-part II: implementation and characterization," J. Microelectromech. Syst. **13**(6), 1054–1062 (2004).
14. D. Weinstein and S. A. Bhave, "Internal dielectric transduction in bulk-mode resonators," J. Microelectromech. Syst. **18**(6), 1401–1408 (2009).
15. T. P. M. Alegre, R. Perahia, and O. Painter, "Optomechanical zipper cavity lasers: theoretical analysis of tuning range and stability," Opt. Express **18**(8), 7872–7885 (2010).

16. R. Perahia, J. D. Cohen, S. Meenehan, T. P. M. Alegre, and O. Painter, "Electrostatically tunable optomechanical 'zipper' cavity laser," Appl. Phys. Lett. **97**(19), 191112 (2010).
17. J. Yao, D. Leuenberger, M. C. M. Lee, and M. C. Wu, "Silicon microtoroidal resonators with integrated mems tunable coupler," IEEE J. Sel. Top. Quantum Electron. **13**(2), 202–208 (2007).
18. K. H. Lee, T. G. McRae, G. I. Harris, J. Knittel, and W. P. Bowen, "Cooling and control of a cavity optoelectromechanical system," Phys. Rev. Lett. **104**(12), 123604 (2010).
19. O. Arcizet, C. Molinelli, T. Briant, P.-F. Cohadon, A. Heidmann, J.-M. Mackowski, C. Michel, L. Pinard, O. Français, and L. Rousseau, "Experimental optomechanics with silicon micromirrors," N. J. Phys. **10**(12), 125021 (2008).
20. S.-S. Li, Y.-W. Lin, Z. Ren, and C. T.-C. Nguyen, "Disk-array design for suppression of unwanted modes in micromechanical composite-array filters," in *19th IEEE International Conference on Micro Electro Mechanical Systems* (2006), pp. 866–869.
21. M. Soltani, S. Yegnanarayanan, and A. Adibi, "Ultra-high Q planar silicon microdisk resonators for chip-scale silicon photonics," Opt. Express **15**(8), 4694–4704 (2007).
22. S. Pourkamali and F. Ayazi, "SOI-based HF and VHF single-crystal silicon resonators with sub-100 nanometer vertical capacitive gaps," in *12th International Conference on Solid-State Sensors, Actuators and Microsystems* (2003), Vol. 1, pp. 837–840.
23. L. Martinez and M. Lipson, "High confinement suspended micro-ring resonators in silicon-on-insulator," Opt. Express **14**(13), 6259–6263 (2006).
24. B. E. Little, S. T. Chu, H. A. Haus, J. Foresi, and J.-P. Laine, "Microring resonator channel dropping filters," J. Lightwave Technol. **15**(6), 998–1005 (1997).
25. X. S. Yao and L. Maleki, "Optoelectronic oscillator for photonic systems," IEEE J. Quantum Electron. **32**(7), 1141–1149 (1996).
26. V. S. Ilchenko, J. Byrd, A. A. Savchenkov, A. B. Matsko, D. Seidel, and L. Maleki, "Miniature oscillators based on optical whispering gallery mode resonators," in *IEEE International Frequency Control Symposiumm* (2008), pp. 305–308.
27. K. H. Lee, T. G. McRae, J. Knittel, and W. P. Bowen, "Laser locking and cavity manipulation with a cavity optoelectromechanical system," IEEE Photon. Technol. Lett. **22**(24), 1784–1786 (2010).
28. M. Hossein-Zadeh and K. J. Vahala, "Photonic RF down-converter based on optomechanical oscillation," IEEE Photon. Technol. Lett. **20**(4), 234–236 (2008).

1. Introduction

Recent work on cavity optomechanics has shown resonators with mechanical displacement sensitivities close to the zero point motion of the mechanical modes [1]. The mechanical motion of these optomechanical resonators is encoded as phase shifts which can be extracted using homodyne detection [1] or by using the optical resonator to convert the phase changes into optical intensity modulation [2]. In addition to offering excellent displacement sensitivities, optical forces have been shown to exist in these optomechanical systems which can be used for a variety of applications including static motion of micro mechanical structures [3,4], excitation of mechanical resonance by modulation of optical input at the mechanical resonant frequency [5], setting up oscillations (heating) of the vibrational modes [2,6–8] and cooling of vibrational modes to achieve ground state [1,2,9,10]. The optomechanical systems can be either stand alone optomechanical resonators on chip which are interrogated by evanescent coupling from fiber taper that provide lower insertion loss [1,2,4,6–8] or on-chip systems which incorporate waveguides along with optomechanical resonators on the same chip [3,5].

Electrostatic capacitive actuation and detection is the main scheme of transduction used in Radio Frequency (RF) Micro Electro Mechanical Systems (MEMS) resonators [11−14]. The use of electrostatics is convenient as it enables direct integration with electronics used for processing RF signals. In electrostatic capacitive actuation, an electric potential is applied between a capacitor constituted by the electrodes surrounding the resonator and the resonator. This field across the capacitor leads to a force on the resonator. A combination of AC and DC potentials are used to obtain a force at a desired frequency. To sense mechanical displacement, the time varying capacitance between the resonator and sense electrodes leads to an AC sense current at the frequency of vibration.

In addition to the two schemes described above, where the actuation and sensing are restricted to the respective domains, it is interesting to consider a crossover scheme where mechanical motion is excited electrically and sensed optically. Electrostatic actuation of optomechanical resonant cavities has been demonstrated earlier for optical resonance tuning [15−17]. Additionally, prior work aimed at electrical actuation of mechanical resonances of

such systems used gradient electrical forces applied through an off-chip electrode on a dielectric resonator [18] and a silicon micromirror [19]. In this work, we present a method for driving an optomechanical resonator using the RF MEMS technique of electrostatic capacitive actuation and sensing of mechanical motion by using the optical intensity modulation at the output of an optomechanical resonator all integrated into a monolithic system fabricated on silicon on insulator (SOI) platform.
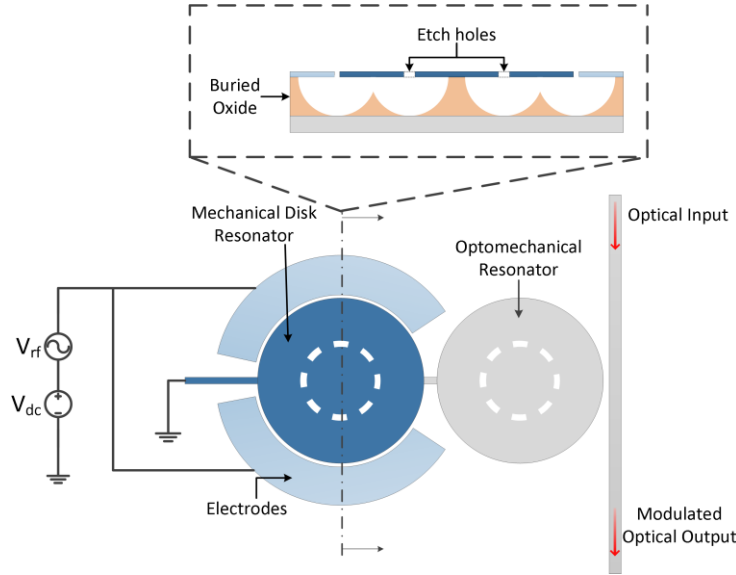
2. Principle of operation

Fig. 1. Schematic of the electrically actuated disk mechanical resonator in blue (on left) coupled to an optomechanical resonator in grey (on right). A combination of DC and RF potential applied to electrodes around the mechanical resonator excite vibrations which get coupled to the optomechanical disk resonator .These radial vibrations affect the optical resonance thereby modulating the intensity of light exiting the waveguide.

Figure 1 shows the schematic of the proposed electrically actuated optomechanical resonator consisting of two suspended microdisk resonators. The microdisk resonator on the left has electrodes around it to provide the electrostatic actuation force for driving mechanical motion. This serves as the driving disk. As the force is proportional to the square of potential across the actuation capacitor, the addition of DC bias results in a force at the RF frequency ω given by $F_{es}(\omega) = (dC/dg)V_{dc}V_{rf}$, where dC/dg is the change in the actuation capacitance (C) for a small change in the electrode to resonator capacitor gap (g). This leads to a radial displacement at the mechanical resonant frequency corresponding to $\Delta r(\omega) = Q_{mech} F_{es}(\omega)/k_{eff}$, where Q_{mech} is the mechanical quality factor and k_{eff} is the effective spring constant of the radial vibrational mode. The disk on the right (colored gray) acts as the optomechanical resonator that senses mechanical motion as a phase shift which causes a variation in its optical resonance frequency. The sensitivity of the optomechanical resonator to radial displacement is obtained from the optical resonance condition $m\lambda_o = 2\pi R n_{eff}$ where m is an integer; n_{eff} is the effective index obtained for the mode and λ_o is free space wavelength. The displacement $\Delta r(\omega)$ gives a shift in optical resonance wavelength of $\Delta\lambda = (\Delta r(\omega)/R)\lambda_o$. For an optical resonance at 1550nm, a radial displacement of 0.5nm of a 10µm radius disk shifts the resonant wavelength by 77.5pm. Continuous wave laser light is input in a waveguide coupled to the optomechanical resonator with wavelength corresponding

to the half maximum point of optical resonance. The mechanical vibration is then detected as an intensity modulation of the output light at the mechanical resonance frequency.

The drive and sense resonators are mechanically coupled through a coupling beam to transfer the vibrations. This prevents the presence of actuation electrodes from degrading the optical quality factor of the optomechanical resonator. This geometry of using mechanically coupled disks is similar to that used in electrostatic capacitive actuation to reduce signal feed through [20]. The coupling beam splits the radial breathing mode of the disk into two modes, one where the motion in the two disks is in phase and one where the motion is out of phase. The combination of the two mechanical modes and the coupling beam result in a filter response to the electrical input with the bandwidth being tunable by the characteristics of the coupling beam.

3. Fabrication

Silicon-on-Insulator (SOI) has been chosen as the system for implementation of the modulator. This is due to the ability to obtain high Q_{opt} optical resonators [21] and high Q_{mech} mechanical resonators [22] with electrical actuation on SOI. The modulator is fabricated using a three mask process on a custom SOI wafer (undoped 250 nm device layer for low optical loss and 3µm thick buried oxide for optical isolation of the waveguides on device layer from the silicon substrate). The top silicon is thermally oxidized to obtain a thin oxide hard mask layer and a silicon device layer thickness of 220nm. Ma-N 2403 electron beam resist is spun on top of the oxide and patterned using electron beam lithography. The patterns are etched into the oxide hard mask on an Oxford System 100 Reactive Ion Etcher (RIE) using CHF3/O_2 chemistry. This pattern is then transferred into the silicon device layer using a chlorine reactive ion etch on a Plasma-Therm 770 RIE to define the modulator, waveguides and bond-pads. A second layer of photoresist is spun and windows are patterned above the mechanical resonator and electrical routing beams. A boron ion implantation is carried out at 30keV with a dose of 2e15 ions/cm and the samples are annealed at 850C to reduce the resistivity of the electrical structures to 0.005Ω.cm. A third mask is then used to pattern release windows near the modulator followed by a timed release etch in buffered oxide etchant to undercut the devices. The samples are dried using a critical point dryer to prevent stiction.
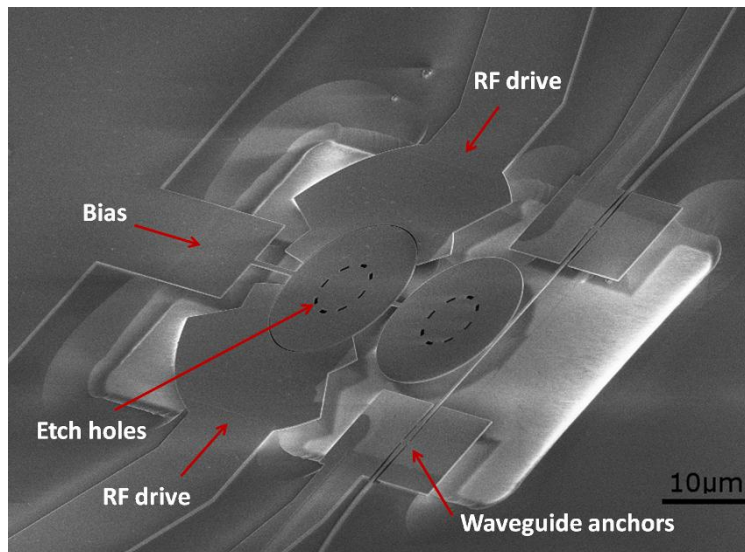

Fig. 2. Scanning electron microscope image of fabricated device showing the coupled disk resonator geometry. The darker silicon shade show the silicon regions where boron has been ion implanted while the lighter silicon regions are undoped silicon.

A scanning electron microscope image of a device fabricated is shown in Fig. 2. The radii of the disks are 10µm which gives a mechanical resonance frequency of 242MHz. The gap between the actuation electrodes and the mechanical resonator is 150nm. The suspended waveguide is anchored to the substrate using tethers to prevent its collapse. S-bend structures are used to reduce the optical loss at these anchor points [23]. Additionally, the disk resonators have etch holes in them to allow the oxide etchant to undercut the disks leaving behind a 1µm diameter pedestal at the center. Grating couplers are used to couple light into and out of the waveguides with a loss of 10.8dB at each coupler.
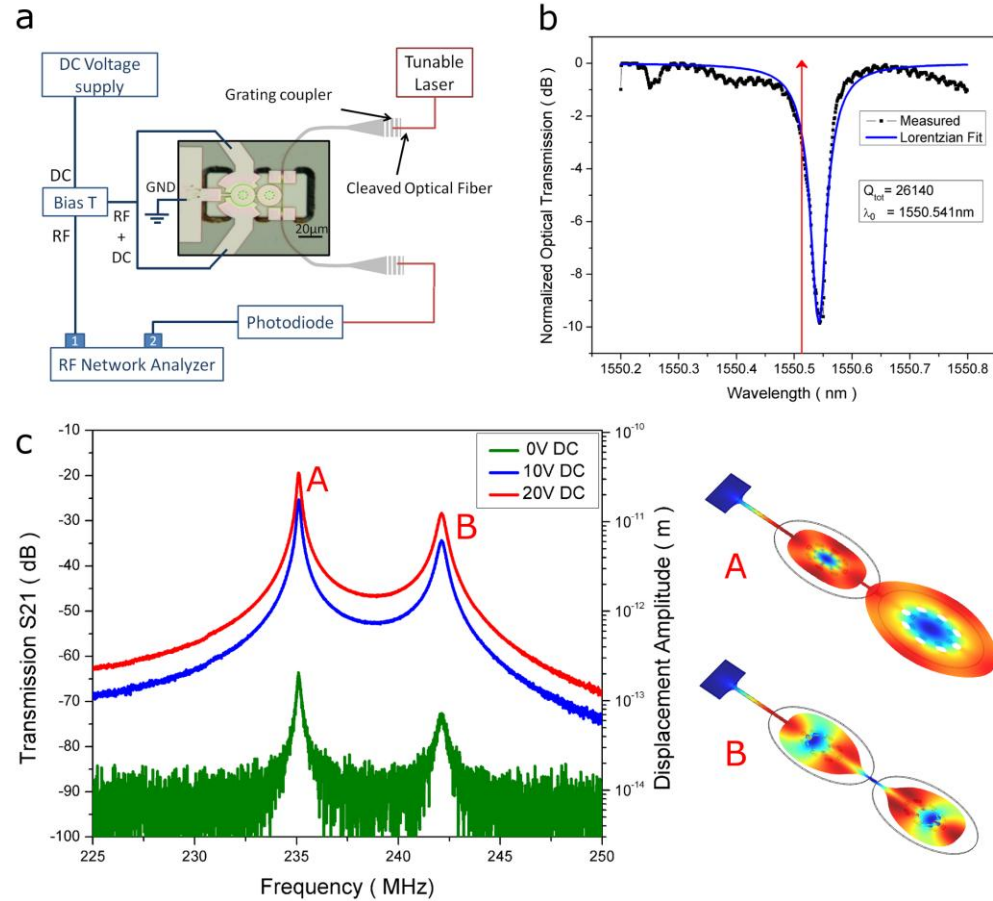
4. Characterization

Fig. 3. a, Setup for measuring the optical response of electrically actuated optomechanical resonators. b, Optical transmission spectrum showing the disk resonance at 1550.541nm with a quality factor of 26,140. The red line shows the wavelength of the tunable laser for the modulator measurements. c, Electrical transmission spectrum observed using the network analyzer showing modulation peaks at 235.1 MHz (A) and 242.1MHz (B) when input RF power is at −10dBm and optical input power is at 6dBm. Inset A and B show the displacement mode shape obtained using finite element method for modes predicted to be at 241.6MHz and 248.3MHz respectively.

To characterize the optical resonator, light from a Santec TSL-510 tunable laser polarized parallel to the substrate is coupled into the waveguide. The optical transmission spectrum shows multiple dips corresponding to the whispering gallery modes of the disk resonator. An optical Q of 26,140 is obtained for a resonance at 1550.541 nm with an extinction of 10 dB as shown in Fig. 3b. To excite mechanical excitations and observe the optical response, a setup

as shown in Fig. 3a. is used. The tunable laser is biased at the half maximum point of the optical resonance and a DC bias along with the RF output from port 1 of an Agilent N5230A network analyzer is applied to the actuation electrodes. The optical output from the gratings is picked up using New Focus 1647 avalanche photodiode with a gain of 4500V/W and sent to port 2 of the network analyzer.

The optical modulation at the mechanical resonant frequency is seen in the S21 plot of the network analyzer in Fig. 3c. The data show that modulation occurs only when the electrical input to the device is around the mechanical resonance frequency of the device. The response shows the presence of two modes of vibration at 235.1 MHz and 242.1 MHz due to splitting of the mechanical mode due to the coupling spring. The mode at 235.1 MHz has a Q_{mech} of 1,300 in air. Increasing the DC voltage results in a larger actuation force and thereby an increase in amplitude of vibration. This leads to larger modulation of optical power for a given input RF power and is seen as a higher value of the transmission (S21). This confirms the hypothesis that the actuation is indeed caused by electrostatics. The predicted mechanical frequencies and the corresponding measured values are in good agreement with each other. In addition to the in phase and out of phase radial vibration modes, we also observe excitation of other vibration modes as shown in Fig. 4.
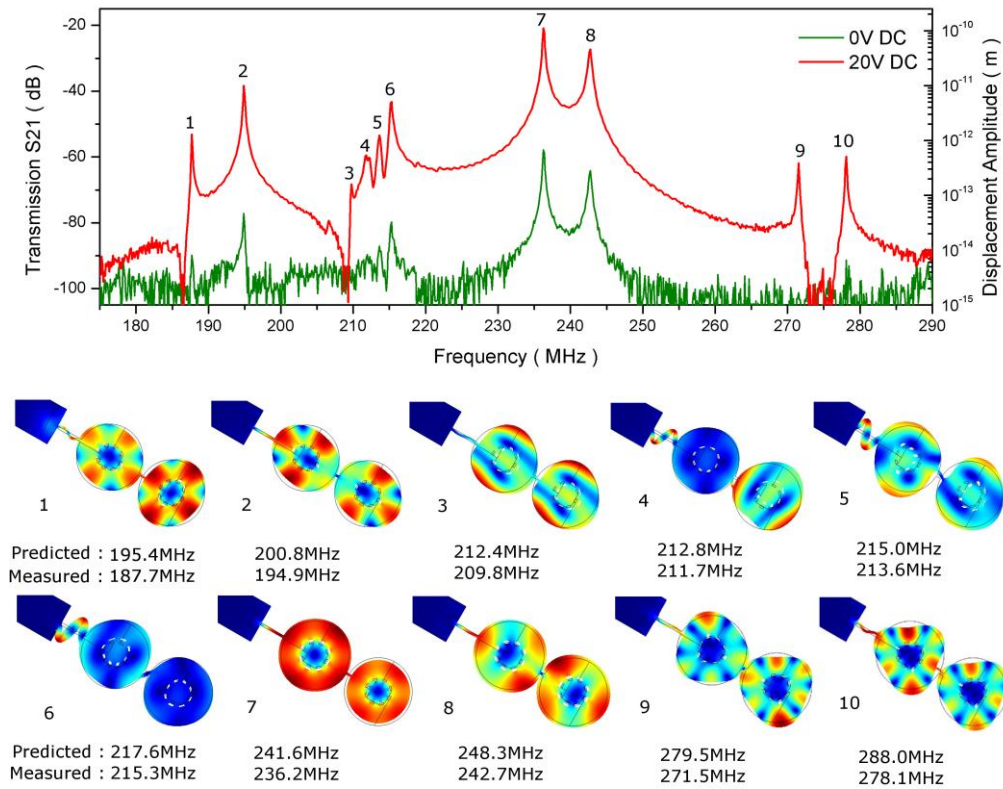

Fig. 4. Transmission spectrum showing modulation at multiple in-plane mechanical resonances for an optical input of 6dBm and a RF input of 0dBm. Insets 1 to 10 show the mechanical mode shape obtained using finite element method and their predicted and measured frequency for modes in the transmission spectrum.

The amplitude of displacement of the disk is calculated by using the modulated power at the network analyzer input. Taking into account the losses, the amplitude of optical power modulation around the average optical power at the bias point for varying RF input and DC bias voltages is shown in Fig. 5. It is seen that the extinction ratio, defined as

$10\log_{10}\left(P_{\max}/P_{\min}\right)$ increases with increasing RF power and DC voltage and is a maximum of 6dB at 15V DC bias and 5dBm RF power. The amplitude of optical modulation for a given radial displacement is obtained by numerically solving the dynamical equation for the optical energy within the optical resonator [2,24]. The calibrated values of radial displacement from these numerical simulations are shown as the alternate y axis on the transmission spectrum of Fig. 3c and Fig. 4. A larger modulation depth can be obtained for the same power and bias voltages by increasing the mechanical quality factor of the disks, which are currently limited by the anchor loss. As there is only one layer to fabricate the resonators and the electrical routing beams, the disk is electrically grounded by a beam that is connected to its edge. This beam is at the maximum displacement point of the radial mode of the disk increasing anchor loss leading to a lower Q_{mech}.
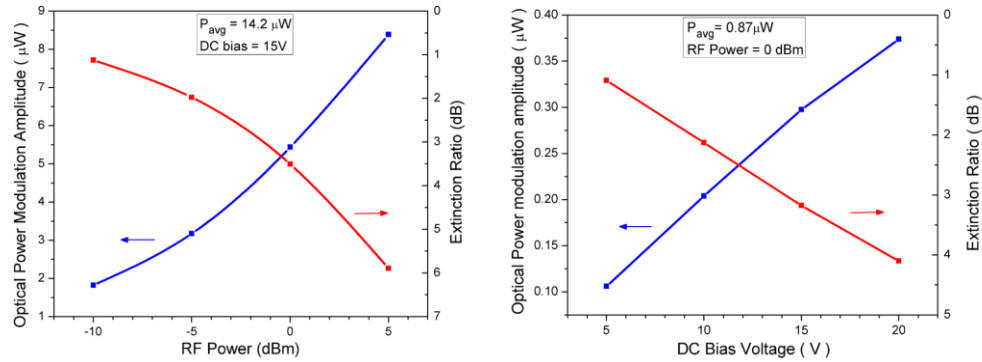

Fig. 5. Variation of the amplitude of optical power modulation and extinction ratio with RF power (left) and DC bias voltage (right) for an optical input power of 6dBm(left) and −6dBm(right).

5. Summary

We have demonstrated a monolithic electrically actuated silicon optomechanical resonator operating at a frequency of 235MHz. There is no DC power dissipated in this device as the DC bias is applied across a capacitor. Since the optical response to the electrical input is shaped by the mechanical transfer function, the device is similar to a RF filter in series with an optical modulator. This device can provide a low-power, on-chip modulator for enabling narrow band applications such as a chip scale implementation of an Optoelectronic Oscillator [25,26]. In its application as narrowband modulator, the device presented in this work can overcome inefficiencies associated with the repeated conversion from electrical → acoustic-filter → electrical → impedance-match → electrical → optical by directly going from electrical → acoustic-filter → optical. This device offers an additional input for controlling the state of an optomechanical system and can be applied in interesting applications of optomechanics such as cooling of mechanical modes [18], in laser locking [27] and RF photonics [28].

Acknowledgments